Applied Physics Express

LETTERS

Photothermal effect in graphene-coated microsphere resonators

Applied Physics Express **11**, 072503 (2018)
https://doi.org/**10.7567/APEX.11.072503**

Photothermal effect in graphene-coated microsphere resonators

Chenzhi Yuan, Wei Zhang*, and Yidong Huang

Tsinghua National Laboratory for Information Science and Technology, Department of Electronic Engineering, Tsinghua University, Beijing 100084, China

*E-mail: zwei@tsinghua.edu.cn

Received April 24, 2018; accepted June 4, 2018; published online June 19, 2018

In this study, graphene-coated silica microsphere resonators with Q values of $\sim 10^5$ are fabricated. After wet transfer of a graphene layer onto the surface of the microsphere, the deterioration of the Q value due to the graphene layer is overcome by a laser treatment. The photothermal effect in the fabricated resonators is investigated experimentally. Using a control-probe scheme, the resonance shift by the photothermal effect is demonstrated, with a high tuning slope. Optical bistability is also observed, with a low threshold and high switching contrast. The experimental results show that the graphene-coated microsphere resonator is a promising platform to investigate the interaction between graphene and light field.

As a type of optical microresonators with whispering gallery modes (WGMs), microsphere resonators have been intensively investigated for various applications, such as ultra-low-threshold lasing,[1,2] bio-sensing,[3,4] nonlinear parametric frequency conversion,[5,6] and optomechanics.[7,8] Their high quality-factor (Q) values provide a large light-field enhancement and long photon lifetime. Therefore, they can significantly enhance the interaction between light and materials. The photothermal effect is an important phenomenon of light–matter interaction.[9–11] The intrinsic photothermal effect in high-Q silica microsphere resonators has been studied.[12–14] These studies showed that the enhanced interaction between the light field and silica leads to the thermal oscillation and dynamical refractive-index modulation in the resonators. In Ref. 15, polymer is coated on a silica microsphere resonator. A photothermal-effect-induced resonance shift has been observed in the resonator, with a significantly larger shift coefficient, compared with those of bare silica microspheres.

Graphene is an atomically thin layer of hexagonally arranged carbon atoms, with various desirable properties.[16–19] Upon interaction with light field, graphene intensively absorbs light and exhibits a strong ohmic self-heating.[20] Using the dry and wet transfer methods, graphene can be integrated into various photonic structures, such as planar waveguides,[20–22] microfibers,[23,24] and some types of microresonators.[25–29] Significant regenerative oscillation and optical bistability have been observed in graphene-coated silicon photonic crystal resonators,[26] silicon ring resonators,[27] and silicon nitride ring resonators,[28] which are based on the enhanced photothermal effect owing to the light absorption in graphene. On the other hand, all-optical resonance control has been demonstrated in a graphene-coated microfiber resonator.[29] However, the reduction of the Q values of microresonators owing to the transferred graphene layers is unavoidable, which limits the combination of graphene and high-Q microresonators, such as microsphere and toroidal ring resonators.

In this study, we fabricated graphene-coated silica microsphere resonators and investigated the photothermal effect. After wet transfer of a graphene layer onto the surface of a microsphere, the deterioration of the Q value due to the graphene layer was reduced by laser treatment. A resonance-frequency shift and bistability due to the photothermal effect were observed in the graphene-coated microsphere resonators, showing that the photothermal effect in the silica microsphere can be significantly enhanced by the graphene layer. This study shows that the graphene-coated microsphere resonator is a promising platform to investigate the interaction between graphene and light field and develop all-optical tunable filter and logic devices.

The microsphere resonator in this study was fabricated on the tip of a silica optical fiber. First, a piece of fiber was tapered to reduce its diameter; an arc discharge process was then applied to its tip, forming a microsphere by the surface tension of the silica material in the molten state.

The graphene transfer process is illustrated in Fig. 1(a). Graphene was transferred from a Cu foil, on which few layers of graphene were grown by chemical vapor deposition (CVD). First, the graphene/Cu foil was put into an $(NH_4)_2S_2O_8$ solution, in which the Cu foil was gradually etched, leaving few layers of graphene in the solution. The graphene layer was then transferred to deionized (DI) water, floating on its surface. In the next step, the graphene layer was transferred to the surface of the microsphere resonator. The graphene layer wrapped the microsphere when it was dipped into the DI water. The graphene was attached to the microsphere, owing to its high hydrophobicity, when the microsphere was removed from the DI water.[30] It was then dried at 100 °C. However, the transferred graphene layer might have folds and overlaps as the surface tension of the DI water could shrink the graphene layer. Figures 1(b) and 1(c) show scanning electron microscopy (SEM) images of the microsphere before and after the graphene transfer. A significant roughness is observed on the microsphere surface after the graphene transfer, owing to the graphene layer.

It is well known that graphene can be easily heated under a strong laser radiation, leading to various changes, such as local decomposition, vaporization, and sublimation.[31,32] This provides an approach to control the loss introduced by graphene. In this study, we introduced a laser treatment to reduce the undesirable effect of the graphene layer on the microsphere. The laser light was coupled into the microsphere by a tapered fiber. The field enhancement of the WGMs was employed to reduce the requirement of light power, which was approximately 80 mW in the laser treatment. The laser light was generated by a telecom-band tunable laser and amplified by an erbium-doped fiber amplifier. The treatment was applied to the microsphere several times using different WGMs. At each treatment, the processing time was approx-

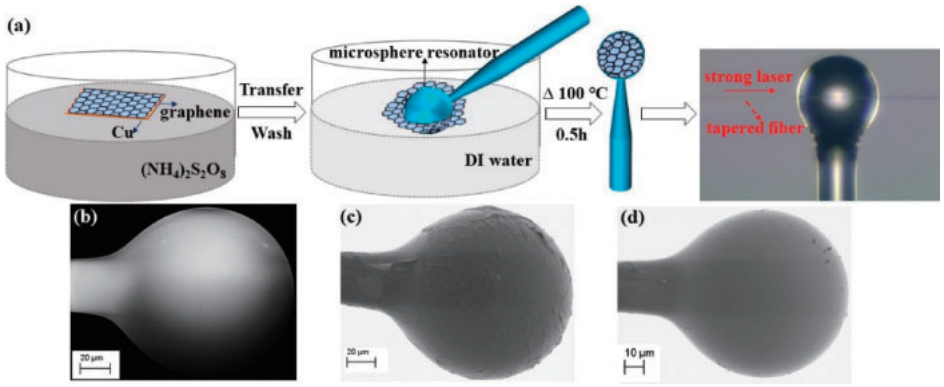

Fig. 1. Fabrication process of the graphene-coated microsphere resonator and SEM images of the microsphere. (a) Fabrication steps. (b–d) SEM images of the bare microsphere, and graphene-coated microsphere before and after the laser treatment, respectively; panels (c) and (d) are secondary-electron images.

imately 8 s. An SEM image of the graphene-coated microsphere resonator after the laser treatment is shown in Fig. 1(d). The laser treatment can significantly reduce the surface roughness introduced by the graphene layer.

The transmission (T) spectrum of the microsphere/tapered-fiber system was measured to evaluate the resonance property of the microsphere resonator. In the measurement, a telecom-band tunable laser was used as the light source, with an output power of 63 μW.

First, the transmission spectrum of the microsphere/tapered-fiber system was measured before the graphene layer was coated on the microsphere; the result is shown in Fig. 2(a). Three groups of resonances appear in the wavelength region of 1580–1590 nm, with a free spectrum region (FSR) of 2.85 nm (the diameter of the microsphere is approximately 200 μm). One group of resonances was measured under a high wavelength resolution, as shown in Fig. 2(b). Several resonances with different wavelengths are excited in this group. The loaded Q of the resonance with the highest extinction ratio is 2.24×10^5, while the intrinsic Q for this resonance is estimated to be 4.5×10^5, close to critical coupling. In order to investigate the material on the microsphere surface, microscopic Raman spectra of the microsphere surface were measured under an excitation laser wavelength of 532 nm (Horiba LabRAM). The result is shown in Fig. 2(c); all of the peaks agree with the characteristic frequency shifts of Raman scattering of silica.

The graphene layer was then transferred onto the microsphere surface by the process shown in Fig. 1(a). The transmission spectrum of the microsphere/tapered-fiber system was measured before the laser treatment, as shown in Figs. 2(d) and 2(e). The resonance dips disappeared and were replaced by small ripples in the spectra. On the other hand, in the typical microscopic Raman spectrum shown in Fig. 2(f), G and 2D peaks with symmetric profiles can be clearly observed at frequency shifts of 1593 and 2683 cm^{-1}, respectively, which are characteristics of the graphene layer. A D peak also appears at 1343 cm^{-1}, attributed to intrinsic defects in the few-layer graphene and broken edges introduced by the transfer process. The microscopic Raman spectra at different locations on the surface are similar with that in Fig. 2(f), showing that the graphene layer wrapped the whole microsphere. It is expected that the disappearance of resonance dips is due to the graphene layer, in particular, due to the surface roughness introduced by the graphene layer.

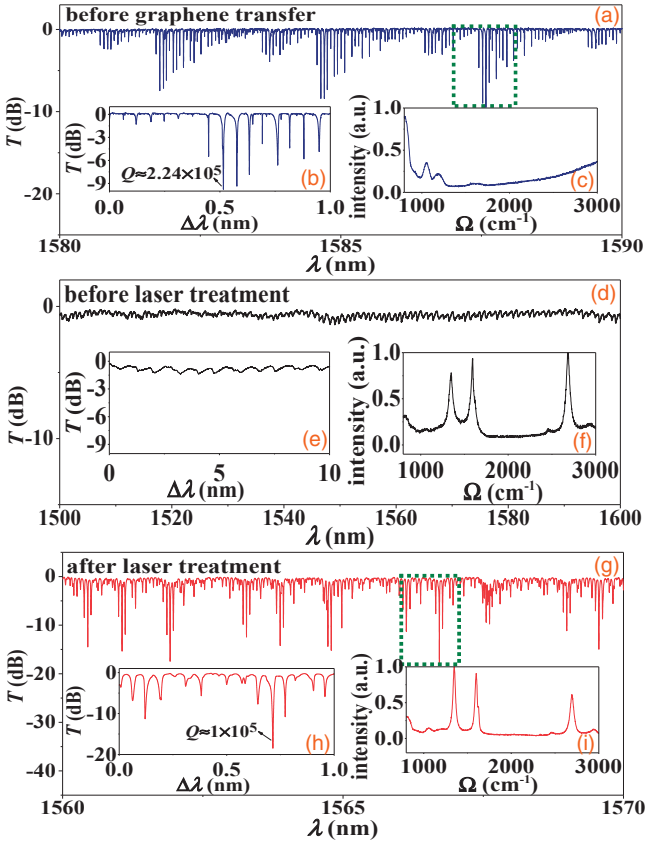

Fig. 2. Measured transmission spectra (T as a function of the wavelength λ) of the microsphere/tapered-fiber system and microscopic Raman spectra (Raman signal intensity as a function of the frequency shift Ω) of the microsphere surface at different steps of the fabrication processes. (a–c) Results of the microsphere resonator without a graphene layer. (d–f) Results of the graphene-coated microsphere resonator before the laser treatment. (g–i) Results of the graphene-coated microsphere resonator after the laser treatment. The wavelength detunings $\Delta\lambda$ in (b), (e), and (h) are relative to 1587, 1545, and 1566 nm, respectively.

Finally, the laser treatment was applied on the microsphere with the graphene layer, and the transmission spectrum of the microsphere/tapered-fiber system was measured again. The results are shown in Figs. 2(g) and 2(h). The resonance dips are recovered, with the same FSR as that in Fig. 2(a). The intrinsic Q of the resonance with the highest extinction ratio is 2×10^5. On the other hand, in the microscopic Raman spectra of the microsphere surface shown in Fig. 2(i),

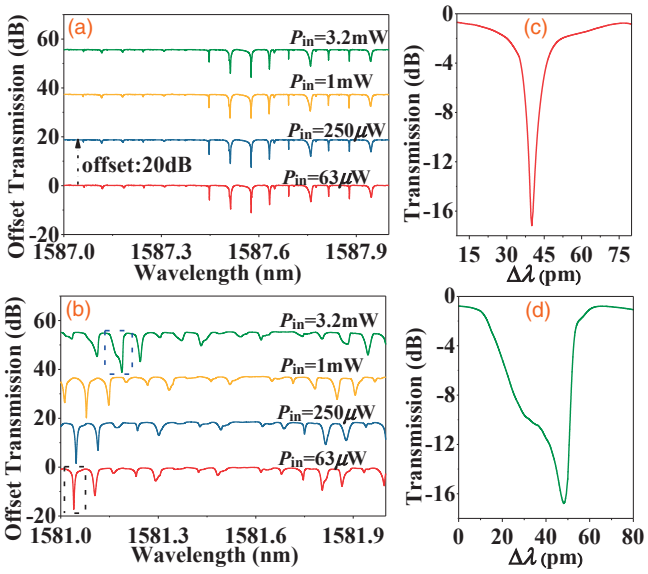

Fig. 3. Measured transmission spectra of the microsphere/tapered-fiber system under different input light powers. Experimental results of the (a) bare microsphere resonator and (b) graphene-coated microsphere resonator after the laser treatment with input powers P_{in} of 63 μW, 250 μW, 1 mW, and 3.2 mW. (c) Details of a specific resonance in (b) under $P_{in} = 63$ μW [indicated in (b) by the black dashed box]. (d) Details of a specific resonance in (b) under $P_{in} = 3.2$ mW [indicated in (b) by the blue dashed box]. The wavelength detunings $\Delta\lambda$ in (b) and (c) are relative to 1581 and 1581.14 nm, respectively.

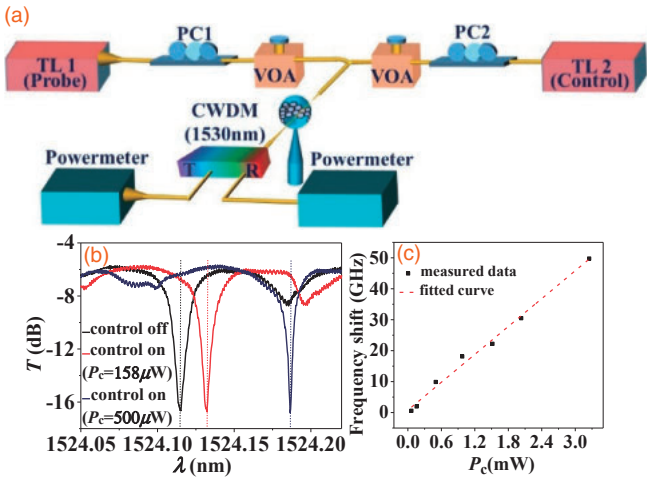

Fig. 4. Experiment setup and results of the control-probe measurement to show the photothermal-effect-introduced resonance-frequency shift. (a) Experimental setup. (b) Transmission spectra of a specific resonance dip under different control light powers. (c) Measured resonance-frequency shifts under different control light powers.

the symmetric G and 2D peaks still exist, showing that the graphene layer is still on the microsphere surface after the laser treatment; the D peak is higher than that in Fig. 2(f), which may be attributed to cracks of the graphene layer introduced by the laser treatment. The microscopic Raman spectra measured at different locations around the sphere were similar to that in Fig. 2(f). These results show that the graphene layer can be preserved after the laser treatment; the intrinsic loss of the graphene-coated microsphere resonator is highly reduced by the laser treatment. Therefore, high-Q resonators could be fabricated with this approach to enhance the interaction between the light field and graphene.

When light is injected into a WGM of the graphene-coated microsphere resonator, the graphene layer absorbs the resonating light and increases the temperature of the silica microsphere by the ohmic self-heating effect. Consequently, the resonance frequencies of the WGMs in the microsphere shift with the temperature variation, mainly due to the refractive-index change with the temperature. This photothermal effect can be observed by the transmission spectrum of the microsphere/tapered-fiber system measured using a tunable laser with a high input light power.

Figures 3(a) and 3(b) show the measured transmission spectra of the bare silica microsphere and high-Q graphene-coated microsphere, respectively, for input powers (P_{in}) of 63 μW, 250 μW, 1 mW, and 3.2 mW. The resonances are almost independent on the input power in the case without the graphene coating; all of the resonance dips of the graphene-coated microsphere remarkably shift to longer wavelengths when P_{in} increases. This comparison shows that graphene introduces a significant photothermal effect to the microsphere resonator.

Details of a specific resonance dip of the graphene-coated microsphere measured under $P_{in} = 63$ μW and $P_{in} = 3.2$ mW are shown in Figs. 3(c) and 3(d), respectively. The dip in Fig. 3(c) has a symmetric shape and can be fitted by a Lorentzian curve. On the other hand, the shape of the resonance dip shown in Fig. 3(c) is asymmetric. Its raising edge is obviously steeper than its falling edge (in the measurement, the light was scanned from shorter wavelengths to longer wavelengths). This is also due to the photothermal effect when the light wavelength was scanned during the measurement.

The results shown in Fig. 3 are not suitable to measure the resonance-frequency shift of WGMs, as the shapes of the resonance dips are deformed by the photothermal effect when they are measured under high light powers. Therefore, we use a control-probe scheme to measure the resonance-frequency shift due to the photothermal effect in the graphene-coated microsphere. The setup is shown in Fig. 4(a).

Two tunable lasers were used to generate probe light (TL1) and control light (TL2). Variable optical attenuators (VOAs) and polarization controllers (PC1 and PC2) were used to adjust their powers and polarizations. They were combined by a fiber coupler and simultaneously injected into the microsphere/tapered-fiber system. The control light was used to excite a specific WGM near 1550 nm under different light powers. Considering the resonance-frequency shift due to the photothermal effect, the wavelength of the control light should be readjusted to ensure its "on-resonance" for each power level. This can be realized by minimizing the output control light from the microsphere/tapered-fiber system. On the other hand, the probe light was scanned to measure another resonance dip near 1524 nm. Its power was set to 63 μW to avoid an additional photothermal effect. When the control light and probe light output from the microsphere/tapered-fiber system, they were separated by an optical filter, which was a coarse wavelength demultiplexing (CWDM) device. They were then measured by power meters.

Figure 4(b) shows typical spectra of the resonance dip measured by the probe light under different control light

powers (P_c). The black dip was observed when the control light was off. The red curve represents the result under $P_c = 158\,\mu W$. A frequency shift of the resonance full-width-at-half-maximum (FWHM) can be realized by such a low control light power. If the control light power increases to $P_c = 500\,\mu W$, a shift of 75 pm is observed. The resonance wavelengths under different control light powers are calculated according to the measured transmission spectra. The relation between the resonance-frequency shift and control light power is shown in Fig. 4(c). The resonance-frequency shift is directly proportional to the control light power. The dashed straight line is their fitting line, with a slope of 15 GHz/mW. The maximum frequency shift is 50 GHz, realized under $P_c = 3.3$ mW. The measured frequency shifts shown in Fig. 4(a) are three orders of magnitude larger than that of the polymer-coated microsphere in Ref. 15. The resonance-frequency shift is repeatable, showing that the photothermal effect of the graphene-coated microsphere has large potentials to realize optical tunable filter and optical switch with a low-power optical control.

Bistability is a common phenomenon in a resonator with photothermal effect. If laser light with a high power is injected into the resonator, the output power of the resonator not only depends on the input power but also is affected by the resonance-frequency shift introduced by the photothermal effect. If the intensity of the input light varies, it becomes a dynamic process. When the input power increases/decreases, the input–output relations of the resonator may be different, leading to bistability. In order to observe the bistability in the graphene-coated microsphere resonator, light with a slowly varying envelope of symmetric triangular wave was injected into the microsphere/tapered-fiber system. It was generated by a tunable continuous-wave (CW) laser and modulated by an acoustic optical modulator (AOM). The period of the triangular wave was 20 s. The output light of the system was detected by a photodetector and recorded by an oscillator. By comparing it with the input light envelope, the input–output relation on the rising edge and falling edge of the triangular envelope can be obtained to show the bistability.

The experimental results are shown in Fig. 5. First, the transmission spectrum of the resonance dip used in the experiment was measured under a low light power of 20 μW, as shown in Fig. 5(a). The measured center wavelength of the resonance was 1574.305 nm. The horizontal axis of Fig. 5(a) represents the relative wavelength detuning with respect to this resonance wavelength. The extinction ratio of the resonance dip is over 10 dB, showing that the resonance is close to critical coupling. The dashed lines in Fig. 5(a) indicate the light wavelengths for the measurements in Figs. 5(b)–5(d).

Figure 5(b) shows the measured input–output relation under a wavelength detuning of $\Delta\lambda = 1$ pm, where the light is almost at resonance. The blue and black curves in the inset figure represent the power evolutions of the input and output lights with time, respectively. The output light evolution is almost symmetric; therefore, the input–output relations on the rising and falling edges are almost the same without bistability. When the wavelength detuning $\Delta\lambda$ increases to 25 pm, an obvious asymmetry appears in the output-light evolution shown in the inset of Fig. 5(c). Consequently, the input–output relations are different with respect to the rising and falling edges, as shown in Fig. 5(c). They behave as a hysteresis loop, which is a characteristic of bistability. The light power for the bistable behavior is in the range of 90 to 160 μW. The maximum switching contrast between the rising and falling branches is approximately 17 dB. Figure 5(d) shows the result when $\Delta\lambda$ increased to 33 pm. Both threshold and power range of the bistability increase with the light power. Compared with previous studies on the photothermal-effect-induced bistability in microresonators coated with graphene,[26–28] the bistability switching contrast realized in this study is one order of magnitude higher, with a lower bistability threshold. This provides a useful platform to investigate complex non-linear dynamic phenomena owing to the photothermal effect and develop all-optical devices with low power consumptions.

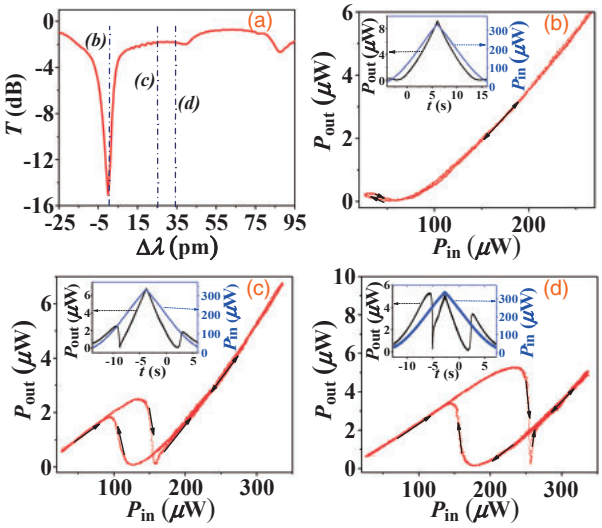

Fig. 5. Photothermal-effect-induced bistability in the graphene-coated microsphere resonator. (a) Transmission spectrum near the resonance used in the measurement; the dashed lines accompanied with italic labels indicate the three input light wavelengths for the results shown in (b–d). The wavelength detuning $\Delta\lambda$ is relative to 1574.305 nm; the transmission spectrum was measured under a low power of 20 μW. (b–d) Input–output relations measured when $\Delta\lambda$ = (b) 1, (c) 25, and (d) 33 pm. The insets in (b–d) show the measured input-(blue)/output-(black) light powers varying with time.

In conclusion, we fabricated graphene-coated silica microsphere resonators with Q values of $\sim 10^5$. After the wet transfer of a graphene layer onto the surface of the microsphere, the deterioration of the Q value due to the graphene layer was overcome by the laser treatment. The photothermal effect in the graphene-coated microsphere resonators was investigated experimentally. By a control-probe scheme, the resonance-frequency shift by the photothermal effect was demonstrated, showing a high tuning slope of 15 GHz/mW. On the other hand, bistability was observed in the resonator, with a low bistability threshold and high switching contrast. These results show that the graphene-coated silica microsphere resonator is a promising platform to investigate the interaction between graphene and light field, and has large potentials for the development of all-optical tunable filter and logic devices.

Acknowledgments This study was supported by the National Key Research and Development Program of China under Contract No. 2017YFA0303700, National Natural Science Foundation of China under Contract Nos. 61575102 and 61621064, and Tsinghua National Laboratory for Information Science and Technology.

1) S. M. Spillane, T. J. Kippenberg, and K. J. Vahala, Nature **415**, 621 (2002).
2) M. Cai, O. Painter, K. J. Vahala, and P. C. Sercel, Opt. Lett. **25**, 1430 (2000).
3) F. Vollmer, S. Arnold, and D. Keng, Proc. Natl. Acad. Sci. U.S.A. **105**, 20701 (2008).
4) M. D. Baaske, M. R. Foreman, and F. Vollmer, Nat. Nanotechnol. **9**, 933 (2014).
5) I. H. Agha, Y. Okawachi, M. A. Foster, J. E. Sharping, and A. L. Gaeta, Phys. Rev. A **76**, 043837 (2007).
6) I. H. Agha, Y. Okawachi, and A. L. Gaeta, Opt. Express **17**, 16209 (2009).
7) R. Ma, A. Schliesser, P. Del'Haye, A. Dabirian, G. Anetsberger, and T. J. Kippenberg, Opt. Lett. **32**, 2200 (2007).
8) Y. S. Park and H.-L. Wang, Opt. Express **15**, 16471 (2007).
9) I. Janossy, J. Mathew, E. Abraham, M. Taghizadeh, and S. Smith, IEEE J. Quantum Electron. **22**, 2224 (1986).
10) R. Shankar, I. Bulu, R. Leijssen, and M. Lončar, Opt. Express **19**, 24828 (2011).
11) V. R. Almeida and M. Lipson, Opt. Lett. **29**, 2387 (2004).
12) Q.-L. Wang, Y. Wang, Z. Guo, J.-F. Wu, and Y.-H. Wu, Opt. Lett. **40**, 1607 (2015).
13) Y. Wang, Q.-L. Wang, S. Zhou, J.-F. Wu, and Y.-H. Wu, Appl. Opt. **54**, 8363 (2015).
14) C. Schmidt, A. Chipouline, T. Pertsch, A. Tünnermann, O. Egorov, F. Lederer, and L. Deych, Opt. Express **16**, 6285 (2008).
15) T. V. Murzina, G. N. Conti, A. Barucci, S. Berneschi, I. Razdolskiy, and S. Soria, Opt. Mater. Express **2**, 1088 (2012).
16) A. H. Castro Neto, F. Guinea, N. M. R. Peres, K. S. Novoselov, and A. K. Geim, Rev. Mod. Phys. **81**, 109 (2009).
17) F. Bonaccorso, Z. Sun, T. Hasan, and A. C. Ferrari, Nat. Photonics **4**, 611 (2010).
18) S. Ghosh, I. Calizo, D. Teweldebrhan, E. P. Pokatilov, D. L. Nika, A. A. Balandin, W. Bao, F. Miao, and C. N. Lau, Appl. Phys. Lett. **92**, 151911 (2008).
19) X. Song, M. Oksanen, J. Li, P. J. Hakonen, and M. A. Sillanpää, Phys. Rev. Lett. **113**, 027404 (2014).
20) Z. Cheng, H. K. Tsang, X. Wang, K. Xu, and J.-B. Xu, IEEE J. Sel. Top. Quantum Electron. **20**, 4400106 (2014).
21) M. Liu, X. Yin, E. Ulin-Avila, B. Geng, T. Zentgraf, L. Ju, F. Wang, and X. Zhang, Nature **474**, 64 (2011).
22) H. Zhou, T. Gu, J. F. McMillan, N. Petrone, A. van der Zande, J. C. Hone, M. Yu, G. Lo, D.-L. Kwong, G. Feng, S. Zhou, and C. W. Wong, Appl. Phys. Lett. **105**, 091111 (2014).
23) X.-T. Gan, C.-Y. Zhao, Y.-D. Wang, D. Mao, L. Fang, L. Han, and J.-L. Zhao, Optica **2**, 468 (2015).
24) W. Li, B.-G. Chen, C. Meng, W. Fang, Y. Xiao, X.-Y. Li, Z. Y. Hu, Y.-X. Xu, L.-M. Tong, H.-Q. Wang, W.-T. Liu, J.-M. Bao, and Y. Ron Shen, Nano Lett. **14**, 955 (2014).
25) X. Hu, Y. Long, M. X. Ji, A. D. Wang, L. Zhu, Z. S. Ruan, Y. Wang, and J. Wang, Opt. Express **24**, 7168 (2016).
26) T. Gu, N. Petrone, J. F. McMillan, A. van der Zande, M. Yu, G. Q. Lo, D. L. Kwong, J. Hone, and C. W. Wong, Nat. Photonics **6**, 554 (2012).
27) C. Horvath, D. Bachman, R. Indoe, and V. Van, Opt. Lett. **38**, 5036 (2013).
28) Y. Gao, W. Zhou, X. K. Sun, H. K. Tsang, and C. Shu, Opt. Lett. **42**, 1950 (2017).
29) Y. Wang, X. Gan, C. Zhao, L. Fang, D. Mao, Y. Xu, F. Zhang, T. Xi, L. Ren, and J. Zhao, Appl. Phys. Lett. **108**, 171905 (2016).
30) J.-H. Chen, W. Luo, Z.-X. Chen, S.-C. Yan, F. Xu, and Y.-Q. Lu, Adv. Opt. Mater. **4**, 853 (2016).
31) M. Currie, J. D. Caldwell, F. J. Bezares, J. Robinson, T. Anderson, H. Chun, and M. Tadjer, Appl. Phys. Lett. **99**, 211909 (2011).
32) B. Krauss, T. Lohmann, D.-H. Chae, M. Haluska, K. von Klitzing, and J. H. Smet, Phys. Rev. B **79**, 165428 (2009).